RSC Advances




ROYAL SOCIETY OF CHEMISTRY

www.rsc.org/advances

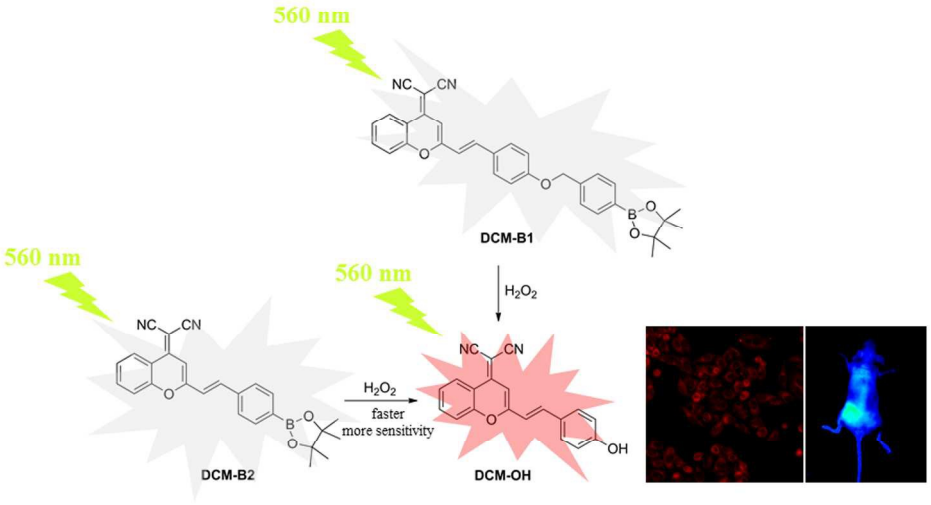


254x190mm (300 x 300 DPI)

# A Novel Colorimetric and Near-infrared Fluorescent Probe for Hydrogen Peroxide Imaging in Vitro and in Vivo

Peng Wang,*[a] Ke Wang,[a] Dan Chen, [a] Yibo Mao, [a] Yueqing Gu [*a]

[a] *Department of Biomedical Engineering, School of Engineering, China Pharmaceutical University, 210009 Nanjing, China*

## Abstract

A novel NIR fluorescent probe DCM-B2 based on dicyanomethylene-4*H*-pyran was synthesized for the detection of $H_2O_2$. This colorimetric fluorescent probe displays fluorescence turn-on response in the process of aryl boronate unit to phenol in the presence of $H_2O_2$. It could offer good performances in terms of sensitivity, selectivity, and low cytotoxicity. Furthermore, bioimaging investigations indicated that this probe was cell permeable and suitable for monitoring $H_2O_2$ in vitro and in vivo.

## Introduction

To date, the reactive oxygen species (ROS) have received considerable attention. ROS as a diverse group of small molecules with different reactivity, sources of production, and, ultimately, biological functions, are important contributors to pathogenesis of major chronic diseases including cancer, diabetes and atherosclerosis. Moreover, some of these molecules play major roles in environmental, radiation and space biology.[1-3]

Among different ROS, the role of $H_2O_2$ as a second messenger, in regulating fundamental biological processes, has been identified not long ago and is increasingly supported by new data.[4] $H_2O_2$ is a non-polar molecule, which can diffuse relatively readily across biological membranes and excerpt its effect in multiple cellular compartments. Due to its low reactivity, $H_2O_2$ also has a relatively long half-life, a feature necessary to carry out long-distance effects across the cell. Escalated level of $H_2O_2$ could be highly harmful, causing oxidative stress through the oxidation of biomolecules, and leading to cellular damage that may become irreversible and cause cell death. It has been reported that when dysfunction, $H_2O_2$ can accumulate and cause oxidative damage to cellular protein, nucleic acids, and lipid molecules, thereby leading to aging and age-related diseases ranging from neurodegeneration to diabetes.[5-7]

Taking advantage of the high sensitivity, noninvasiveness and high spatiotemporal resolution for visualizing bioactive species in a biological system, fluorescence probes are the preferred methods to elucidate the mechanisms of these species. Fluorescent $H_2O_2$ probes, designed to detect this oxygen metabolite with high selectivity, are powerful tools for real-time, noninvasive monitoring of $H_2O_2$ chemistry in biological specimens.

Recently, a few metal-mediated fluorescent probes have been developed for the detection of $H_2O_2$.[8] However, the above-mentioned fluorescent probes are not applicable to be used in biological systems due to slow response time or incompatibility with biological milieus. Compared to most other conventional

fluorescent probes, those that rely on Near-infrared (NIR) fluorescence possess unique advantages for tracing molecular processes *in vitro* and *in vivo*.[9] NIR photons can penetrate tissues more deeply and avoid background noise. Therefore, it would be desirable to utilize NIR fluorophores as the signaling subunit in probes. At present, most of the fluorophores used for $H_2O_2$ probes, such as xanthenones,[10] naphthalenes,[11] and Peroxy Crimson,[12] suffer from short wavelength emission. There is a still lack of probe detecting $H_2O_2$ *in vivo* and *in situ*, which is most probably ascribed to the poor photostability of fluorophores. Moreover, the other challenges to detect $H_2O_2$ using fluorescence probes include chemoselectivity, the selectivity of $H_2O_2$ over other ROS, and bioorthogonality, without interfering with intrinsic cellular biochemistry.

To solve the above problems, we invested effort into developing novel NIR fluorescent probes for $H_2O_2$ detection. As donor-π-acceptor (D-π-A) structured chromophore, dicyanomethylene-4*H*-pyran (DCM) derivatives have attracted considerable attention owing to their attractive features such as controllable emission wavelength in the NIR region *via* tuning electron donor ability, large Stokes shift from the ultrafast intramolecular charge transfer (ICT), and high photostability.[13-15] In addition, some studies establish that $H_2O_2$ can react with aryl boronates to achieve selectivity over other ROS. And the reaction of $H_2O_2$ with boronates is faster than those of the corresponding alkyl peroxides, making the reaction of free $H_2O_2$ selective over lipid-derived peroxides.[16] This reaction may provide a promising opportunity for $H_2O_2$ detection chemically.

In the current study, novel NIR probes based DCM were designed for visualization of $H_2O_2$ in cells and *in vivo*. As shown in **Scheme 1**, the DCM-B1 was constructed by introducing a boronate-based self-immolative linker to DCM-OH, which has been successfully utilized in cell imaging.[17] While DCM-B2 was designed by installation of boronic ester group at the 4'-position of benzene ring, which can react with $H_2O_2$ to release DCM-OH.

## Experimental

### General

All solvents and other reagents were of commercial quality and used without further purification. UV-Vis Spectrophotometer (JH 754PC, Shanghai, China) was used for the absorption measurements. PerkinElmer LS55 was utilized for fluorescence spectra detection. Laser confocal fluorescence microscopy (FluoView$^{TM}$, FV1000, Olympus, Japan) was used for cell imaging. IR spectra were measured using a Bruker Tensor-27 FRIR spectrometer using the KBr pellet. $^{1}$H-NMR and $^{13}$C-NMR spectra were taken on Bruker Advance 300-MHz spectrometer, δ values are in ppm relative to TMS. Mass data (ESI) were recorded by quadruple mass spectrometry. For the $H_2O_2$ selectivity experiments, $H_2O_2$, TBHP and hypochlorite (NaClO) were delivered from 30%, 70% and 5% aqueous solutions, respectively. Superoxide ($O_2^-$) was added as solid $KO_2$. HO· and *t*-BuO· were generated by reaction of 1 mM $Fe^{2+}$ with 100 mM $H_2O_2$ or 100 mM *tert*-butyl hydroperoxide (TBHP), respectively. NO was added using NO gas. Singlet oxygen ($^1O_2$) was generated from the thermodissociable endoperoxide of disodium 3,3'-(1,4-naphthalene)bispropionate.

**Synthesis of DCM-OH**

2-(2-methyl-4*H*-chromen-4-ylidene)malononitrile (1.0 mmol) and 4-hydroxybenzaldehyde (1.0 mmol) were dissolved in 10 mL anhydrous ethyl alcohol. Then piperidine (4.0 mmol) was added and heated to reflux for 5 h. The mixture was cooled to room temperature and filtered to obtain red solid DCM-OH in 80% yield. $^{1}$H-NMR (300 MHz, DMSO-*d6*): δ 10.12 (s, 1H), 8.66 (d, *J* = 7.4 Hz, 1H), 7.86 (s, 1H), 7.71 (d, *J* = 7.6 Hz, 1H), 7.57 (m, 4H), 7.18 (d, *J* = 15.9 Hz, 1H), 6.86 (m, 3H). $^{13}$C-NMR (75 MHz, DMSO-d6): δ 159.9, 158.7, 152.6, 151.9, 139.1, 135.1, 130.3, 126.0, 125.9, 124.5, 118.9, 117.3, 117.0, 116.0, 115.8, 105.6, 59.1. ESI-MS: 311.0 $[M-H]^-$.

**Synthesis of DCM-B1**

The compound 2-(4-(bromomethyl)phenyl)-4,4,5,5-tetramethyl-1,3,2-dioxaborolane (1.1 mmol) and DCM-OH (1.0 mmol) were dissolved in 10 mL $CH_3CN$. Then $K_2CO_3$ (2.0 mmol) was added under nitrogen atmosphere, and was heated to 70 $^{o}$C for 3 h. After cooling, the solid was removed by filtration and washed with $CH_3CN$. The solution was concentrated on a rotary evaporator. The resultant crude material was

recrystallized by ethyl alcohol to afford compound DCM-B1 in 70% yield. $^{1}$H−NMR (300MHz, DMSO-*d6*): δ 8.72 (d, *J* = 8.2 Hz, 1H), 7.91 (t, *J* = 7.8 Hz, 1H), 7.78-7.67 (m, 6H), 7.59 (t, *J* = 7.7 Hz, 1H), 7.47 (d, *J* = 7.6 Hz, 2H), 7.34 (d, *J* = 16.0 Hz, 1H), 7.10 (d, *J* = 8.4 Hz, 2H), 6.96 (s, 1H), 5.22 (s, 2H), 1.30 (s, 12H). $^{13}$C-NMR (75 MHz, DMSO-d6): δ 160.1, 158.5, 152.8, 151.9, 140.0, 138.5, 135.3, 134.5, 130.0, 127.8, 126.8, 126.0, 124.6, 119.0, 117.2, 117.2, 117.1, 115.9, 115.4, 106.0, 83.6, 69.2, 59.5, 24.6. IR (KBr): 2974, 2211, 2198, 1628, 1592, 1501, 1478, 1410, 1357, 1321, 1211, 1170, 1140, 1087, 977, 854, 813, 742, 651 $cm^{-1}$.

**Synthesis of DCM-B2**

2-(2-methyl-4*H*-chromen-4-ylidene)malononitrile (1.0 mmol) and 4-(4,4,5,5-tetramethyl-1,3,2-dioxaborolan-2-yl)benzaldehyde (1.0 mmol) were dissolved in 10 mL anhydrous ethyl alcohol. Then piperidine (4.0 mmol) was added and heated to reflux for 5 h. The mixture was cooled to room temperature and filtered to obtain yellow solid DCM-B2 in 78% yield. $^{1}$H-NMR (300MHz, $CDCl_3$): δ 8.93 (d, *J* = 8.2 Hz, 1H), 7.88 (d, *J* = 7.8 Hz, 2H), 7.75 (t, *J* = 7.8 Hz, 1H), 7.62 (m, 4H), 7.46 (t, *J* = 7.7 Hz, 1H), 6.90 (t, *J* = 8.0 Hz, 2H), 1.36 (s, 12H). $^{13}$C-NMR (300 MHz, DMSO-*d6*): δ 157.5, 152.6, 151.8, 137.8, 137.4, 135.2, 134.7, 127.2, 125.9, 124.5, 120.7, 118.8, 116.8, 116.7, 115.4, 107.0, 83.6, 24.5. IR (KBr): 3067, 3028, 2975, 2209, 1634, 1500, 1460, 1327, 1262, 1089, 1016, 765, 740, 651, 618 $cm^{-1}$.

**Cell culture and confocal fluorescence imaging**

The human cell lines MCF-7 (breast cancer cells) was purchased from American Type Culture Collection (ATCC; Manassas, VA, USA). Cells were cultured in DMEM (Invitrogen) supplemented with 10% fetal bovine serum (FBS, Hyclone), 100 μg/mL penicillin and 100 μg/mL streptomycin at 37 $^{o}$C in a humidified atmosphere containing 5% $CO_2$. One day before imaging, cells were seeded in laser scanning confocal microscope (LSCM) culture dishes with a density of $5\times10^5$ cells per well. The dishes were subsequently incubated at 37 $^{o}$C in a humidified atmosphere containing 5% $CO_2$. Then the cells were incubated with 10 μM DCM-B2 for 30 min. Subsequently, 100 μM $H_2O_2$ was added and incubated at 37 $^{o}$C for 30 min. The cells were washed three times with Dulbecco's PBS (pH 7.0) to remove free compound

before analysis. MCF-7 cells only incubated with 10 μM DCM-B2 for 30 min acted as a control. Confocal luminescence images of MCF-7 cells were carried out on an Olympus FV1000 laser scanning confocal microscope.

**Cytotoxic assay**

MCF-7 cells were seeded in a 96-well plate ($1\times10^4$ cells/well). After cultivation for 24 h, DCM-B2 (DMSO dissolve first, then added it into the cell culture medium) of different concentrations were added into the wells (n = 6) and incubated for 48 h. Then stock solution of MTT (20 μl; 5 mg/ml) was added into each well. After 4 h incubation at 37 $^{o}$C, the MTT solution was replaced with 150 μl DMSO in each well. The absorbance in each well was measured at 570 nm with a multi-well plate reader. Cell viability was calculated using the following formula: Cell viability = (Mean absorbance of test wells - Mean absorbance of medium control wells) / (Mean absorbance of untreated wells - Mean absorbance of medium control well) × 100%.

**Fluorescent imaging in living mice**

Athymic nude mice were purchased from Charles River Laboratories (Shanghai, China) for *in vivo* imaging investigation. All animal experiments were carried out in compliance with the Animal Management Rules of the Ministry of Health of the People's Republic of China (Document no. 55, 2001) and the guidelines for the Care and Use of Laboratory Animals of China Pharmaceutical University. Athymic nude mice, 5-10 g, were selected and divided into two groups. The mice were given an s.p. (skin-pop) injection of probe DCM-B2 (100 μM, in DMSO/saline = 1:9, v/v) on the back of Nude mice. Then one group the mice were injected with 2 mM hydrogen peroxide at the same region. The other group was given saline as the control. Images were taken after incubation for 30 min by using the NIR fluorescence imaging system. This home-built imaging system was reported in our previous works.[18-20] The NIR system contains an excitation laser (λ = 660 nm), a high sensitivity NIR CCD camera (PIXIS 512B, Princeton Instrumentation) and a 700 nm long pass filter for capturing the fluorescence emission from the tissue.

## Results and discussion

**Synthesis of DCM-B1 and DCM-B2**

According to the synthetic route shown in **Scheme 2**, DCM-B1 was prepared in two reaction steps and obtained as the yellow solid in a reasonable yield.[21, 22] Similarly, DCM-B2 was obtained in good yield by the reaction between 2-(2-methyl-4*H*-chromen-4-ylidene)malononitrile with 4-(4,4,5,5-tetramethyl-1,3,2-dioxaborolan-2-yl)benzaldehydes. The structures of DCM-B1 and DCM-B2 were characterized using NMR and mass spectrometry from which satisfactory results corresponding to its structure were obtained. Both of them are soluble in common organic solvent such as DMSO, acetonitrile and dichloromethane, but slightly soluble in water.

**UV-vis and fluorescence responses**

We evaluated the optical properties of DCM-B1 and DCM-B2 in PBS buffer (20 mM, 50% DMSO, pH 7.4). DCM-B1 features one prominent absorption band in the visible region centered at 450 nm and one weak absorption band at around 550 nm (**Figure S1**). DCM-B1 shows weak fluorescence with an emission maximum at 560 nm. Similarly, DCM-B2 has two absorptions maximum at around 420 nm and 450 nm, with a corresponding weak emission band centered at 560 nm (**Fig. 1**). After treatment DCM-B1 and DCM-B2 with $H_2O_2$ for 30 min, a new absorption peak appeared at 560 nm for these two probes. Notably, the red-shift of 110 nm in the absorption is very large with respect to that of other $H_2O_2$ chemosensors, allowing the capacity of DCM-B1 and DCM-B2 for colorimetric detection of $H_2O_2$ even with the naked eyes.

Probe DCM-B1 and DCM-B2 showed almost no fluorescence emission upon excitation at 560 nm. Addition of $H_2O_2$ resulted in marked increase in red fluorescence for DCM-B1 and DCM-B2 (**Fig. 2a**, **S2**). With increasing concentrations of $H_2O_2$, the fluorescence titration curve showed a steady and smooth enhancement. Reaction of DCM-B1 with $H_2O_2$ triggered almost 30-fold fluorescence turn-on, whereas $H_2O_2$ elicited a 50-fold increase in fluorescence for DCM-B2. Absorption and emission spectra, along with mass spectrometry data, establish that the $H_2O_2$-mediated boronate deprotection of DCM-B1 and DCM-B2 generate DCM-OH as fluorescence product. Upon addition of $H_2O_2$, the fluorescence intensity of

DCM-B1 and DCM-B2 enhanced apparently with a maximum at 700 nm, indicating both of these two probes were suitable for application in cells and *in vivo*. These results indicated that DCM-B1 and DCM-B2 were turn-on type fluorescent probes for $H_2O_2$ detection.

To further confirm the sensitivity of the probe, the fluorescence of the probes were measured by adding diverse concentrations of $H_2O_2$. Figure suggested that the fluorescence intensity of probe DCM-B1 and DCM-B2 increased following the increased concentration of $H_2O_2$ within a certain range. There was a good linearity between relative fluorescent intensity at 700 nm and the concentration of $H_2O_2$ ranging from 0-150 μM (**Fig. 2b**, **S3**). The regression equation was $F_{700nm}$ = 4.1993 [$H_2O_2$] (μM) +26.319 ($r$ = 0.9959). The detection limit of $H_2O_2$ was calculated from the equation DL = 3σ/S, where σ is the standard deviation of blank measurement, S is the slope between intensity versus sample concentration.[23] The detection limit of DCM-B1 toward $H_2O_2$ was calculated to be $7.9\times10^{-8}$ M, suggesting that DCM-B1 was highly sensitive to $H_2O_2$. Similarly, the regression equation of DCM-B2 was $F_{700nm}$ = 4.7851 [$H_2O_2$] (μM) +21.624 ($r$ = 0.9937). The detection of DCM-B2 for $H_2O_2$ was $3.9\times10^{-8}$ M, indicating that DCM-B2 was more sensitivity than DCM-B1. These results indicated that the probe DCM-B2 can be used to quantify the concentration of $H_2O_2$.

The time-dependent fluorescence changes of DCM-B1 and DCM-B2 were also investigated (**Fig. 3**). As shown in **Fig. 3c**, the response time of DCM-B2 was shorter than it of DCM-B1, which indicated that the reaction rate between DCM-B2 and $H_2O_2$ was faster than DCM-B1. It might be due to the boronic ester group at DCM-B2 attack by $H_2O_2$ to release DCM-OH directly, while DCM-B1 needs the self-immolative process.

**$H_2O_2$ selectivity**

For an excellent probe, high selectivity is a very important parameter. We next examined the selectivity of DCM-B1 and DCM-B2 towards $H_2O_2$ across a series of other related reactive oxygen species in biological systems. DCM-B1 and DCM-B2 were respectively incubated with various biologically relevant species including

hydroxyl radical (OH•), *t*-butoxy radical (*t*-BuO•), superoxide anion ($O_2^-$), *t*-butyl hydroperoxide (TBHP), hypochlorite ($ClO^-$), singlet oxygen ($^1O_2$), nitric oxide (NO). As a result, only $H_2O_2$ induced a remarkable fluorescence enhancement with an excitation at 560 nm. **Fig. 4** exhibited that addition of $H_2O_2$ presented a 30-fold increase than the control in fluorescence intensity at 30 min. However, there was little to no increase in intensity when the probe reacted with the other ROS over an hour. These results indicated that DCM-B2 has the reasonable activity and selectivity to identify $H_2O_2$ in a complex biological environment. Although DCM-B1 also has good selectivity to identify $H_2O_2$ (**Fig. S4**), DCM-B2 has better detection limit, faster reaction rate, and lower background noise than DCM-B1. Hence, the following experiments were focused on the probe DCM-B2 for visualization of $H_2O_2$ in cells and *in vivo*.

**Fluorescence imaging and cytotoxic assay**

Next, we investigated the ability of DCM-B2 to detect $H_2O_2$ in living cells. Initially, MCF-7 cells were incubated with 10 μM DCM-B2 for 30 min at 37 $^oC$. As control, the cells exhibited almost no fluorescence (Figure 5a). Bright-field measurements after the treatment with DCM-B2 confirmed that the cells were viable throughout the imaging experiments (**Fig. 5b**, **5c**). By contrast, when incubated with 100 μM $H_2O_2$ for 30 min after treat with DCM-B2, the cells displayed obvious fluorescence (**Fig. 5e**). Overlays of confocal fluorescence and bright-field images demonstrated that the fluorescence was evident (**Fig. 5f**). Therefore, these results indicated that DCM-B2 is cell membrane-permeable and available for detection of $H_2O_2$ in living cells.

Moreover, the cytotoxicity of DCM-B1 was evaluated using cell viability assay. MCF-7 cells were treated with different concentrations of DCM-B1 (from 10 to 100 μM) for 24 h, and then cell viability was evaluated by MTT assay. The results showed that cell viability was over 85% even though 100 μM DCM-B2 was added for 24 h, indicating that the fluorescence probe DCM-B2 had low cytotoxicity (**Fig. S5**). The above experimental results proved that DCM-B2 could offer good performances in terms of sensitivity, selectivity, and low cytotoxicity.

**Fluorescent imaging *in vivo***

We further applied DCM-B2 for $H_2O_2$ imaging in the nude mice. The back of mice were injected with 100 μM DCM-B2 (100 μL in 1:9 DMSO/saline v/v), and 10 min later, these were injected with 2 mM $H_2O_2$ (100 μL in saline) in the same region. After 30 min, there was a remarkable increase in fluorescence in the injection region (**Fig. 6b**). As control, the other group of mice were only injected with 100 μM DCM-B2 (100 μL in 1:9 DMSO/saline, v/v) and imaged after 40min. The control showed only slight fluorescence (**Fig. 6a**). These results showed that the NIR fluorescent probe DCM-B2 could be successfully applied for deep imaging in live mice and effectively avoid organisms' autofluorescence. The quantification of mean fluorescence intensity of each group is shown in **Fig. 6c**. It is noteworthy that the total number of photons from the interest region was 3-fold that of control. The above experiments demonstrated that DCM-B2 achieved noninvasive imaging in living mice and was sensitive enough to visualize $H_2O_2$ in living animals.

## Conclusions

In summary, novel NIR fluorescent probes DCM-B1 and DCM-B2 were designed and synthesized. These probes can detect $H_2O_2$ with a fluorescence turn-on effect, and the detection limits are $7.9\times10^{-8}$ M and $3.9\times10^{-8}$ M, respectively. Moreover, DCM-B2 exhibits high selectivity, good sensitivity and low cytotoxicity in the detection of $H_2O_2$. We confirm that DCM-B2 can detect $H_2O_2$ in mice without interference from background fluorescence. The probe DCM-B2 may present a promising tool to detect $H_2O_2$ during the physiological and pathological processes.

## Acknowledgements

We are grateful for the financial support from the NSFC (National Nature Science Foundation of China, No. 81501529) and Fundamental Research Funds for the Central Universities (ZJ15011).

## Notes and references

1. S. V. Chetyrkin, M. E. Mathis, A. J. L. Ham, D. L. Hachey, B. G. Hudson and P. A. Voziyan, *Free Radical Bio Med*, 2008, **44**, 1276-1285.

2. M. Diehn, R. W. Cho, N. A. Lobo, T. Kalisky, M. J. Dorie, A. N. Kulp, D. L.

Qian, J. S. Lam, L. E. Ailles, M. Z. Wong, B. Joshua, M. J. Kaplan, I. Wapnir, F. M. Dirbas, G. Somlo, C. Garberoglio, B. Paz, J. Shen, S. K. Lau, S. R. Quake, J. M. Brown, I. L. Weissman and M. F. Clarke, *Nature*, 2009, **458**, 780-U123.

3. P. D. Ray, B. W. Huang and Y. Tsuji, *Cell Signal*, 2012, **24**, 981-990.
4. H. C. Guo, H. Aleyasin, B. C. Dickinson, R. E. Haskew-Layton and R. R. Ratan, *Cell Biosci*, 2014, **4**, 64.
5. Y. H. A. Liu and X. B. Liao, *Curr Org Chem*, 2013, **17**, 654-669.
6. T. Finkel, M. Serrano and M. A. Blasco, *Nature*, 2007, **448**, 767-774.
7. J. B. Pi, Y. S. Bai, Q. Zhang, V. Wong, L. M. Floering, K. Daniel, J. M. Reece, J. T. Deeney, M. E. Andersen, B. E. Corkey and S. Collins, *Diabetes*, 2007, **56**, 1783-1791.
8. D. Song, J. M. Lim, S. Cho, S. J. Park, J. Cho, D. Kang, S. G. Rhee, Y. You and W. Nam, *Chem Commun*, 2012, **48**, 5449-5451.
9. Z. Q. Guo, S. Park, J. Yoon and I. Shin, *Chem Soc Rev*, 2014, **43**, 16-29.
10. M. C. Y. Chang, A. Pralle, E. Y. Isacoff and C. J. Chang, *J Am Chem Soc*, 2004, **126**, 15392-15393.
11. C. Chung, D. Srikun, C. S. Lim, C. J. Chang and B. R. Cho, *Chem Commun*, 2011, **47**, 9618-9620.
12. E. W. Miller, O. Tulyanthan, E. Y. Isacoff and C. J. Chang, *Nat Chem Biol*, 2007, **3**, 263-267.
13. X. M. Wu, X. R. Sun, Z. Q. Guo, J. B. Tang, Y. Q. Shen, T. D. James, H. Tian and W. H. Zhu, *J Am Chem Soc*, 2014, **136**, 3579-3588.
14. Z. Q. Guo, W. H. Zhu and H. Tian, *Chem Commun*, 2012, **48**, 6073-6084.
15. W. Zhu, X. M. Huang, Z. Q. Guo, X. M. Wu, H. H. Yu and H. Tian, *Chem Commun*, 2012, **48**, 1784-1786.
16. A. R. Lippert, G. C. Van de Bittner and C. J. Chang, *Acc Chem Res*, 2011, **44**, 793-804.
17. D. H. Yu, Q. Zhang, S. S. Ding and G. Q. Feng, *Rsc Adv*, 2014, **4**, 46561-46567.

18. H. Y. Chen, S. N. Wan, F. X. Zhu, C. Wang, S. S. Cui, C. L. Du, Y. X. Ma and Y. Q. Gu, *Contrast Media Mol I*, 2014, **9**, 122-134.
19. H. Y. Chen, M. Zhang, H. B. Yang, W. X. Xu, Y. X. Ma and Y. Q. Gu, *Rsc Adv*, 2014, **4**, 8191-8199.
20. X. Li, D. W. Deng, J. P. Xue, L. Z. Qu, S. Achilefu and Y. Q. Gu, *Biosens Bioelectron*, 2014, **61**, 512-518.
21. E. J. Na, K. H. Lee, Y. K. Kim and S. S. Yoon, *Mol Cryst Liq Cryst*, 2012, **568**, 8-14.
22. W. Sun, J. L. Fan, C. Hu, J. F. Cao, H. Zhang, X. Q. Xiong, J. Y. Wang, S. Cui, S. G. Sun and X. J. Peng, *Chem Commun*, 2013, **49**, 3890-3892.
23. J. Zhou, Y. Li, J. N. Shen, Q. Li, R. Wang, Y. F. Xu and X. H. Qian, *Rsc Adv*, 2014, **4**, 51589-51592.

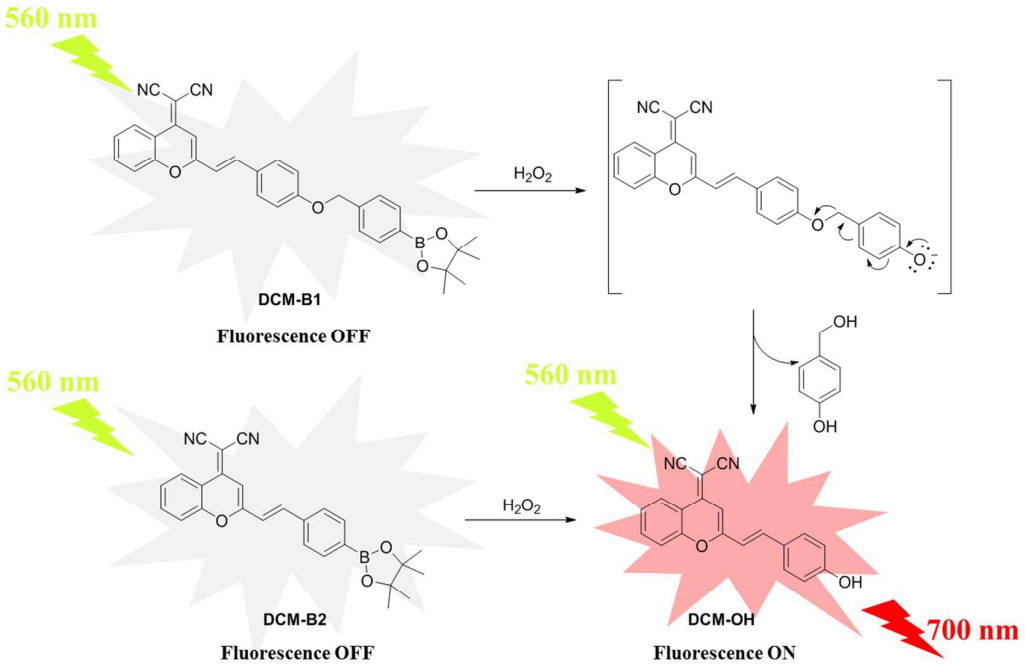


**Scheme 1** The structure and the reaction mechanism of the probe DCM-B1 and DCM-B2.

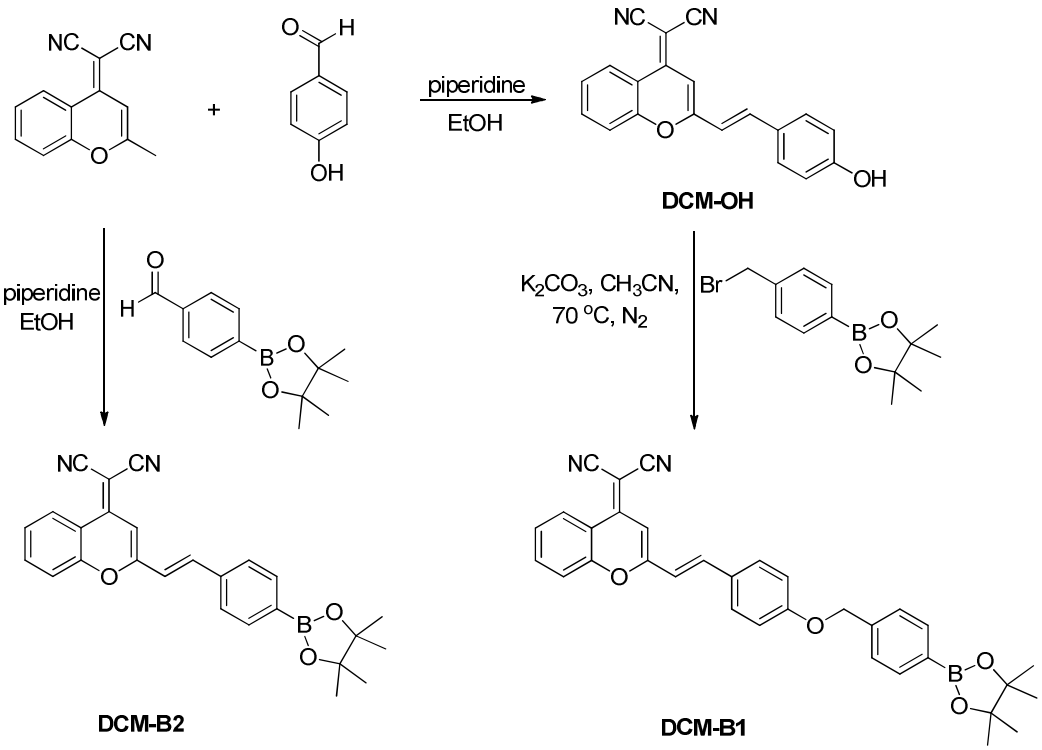


**Scheme 2** The synthetic route of probe DCM-B1 and DCM-B2

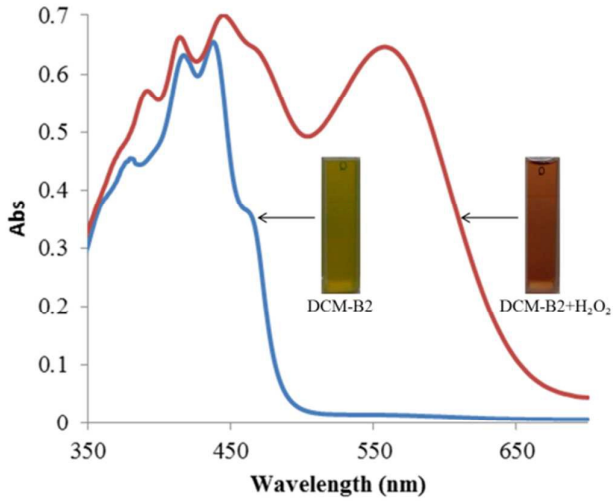


**Fig. 1** Absorption spectra of probe DCM-B2 (5 μM) before (blue line) and after reacting with $H_2O_2$ (100 μM, red line).

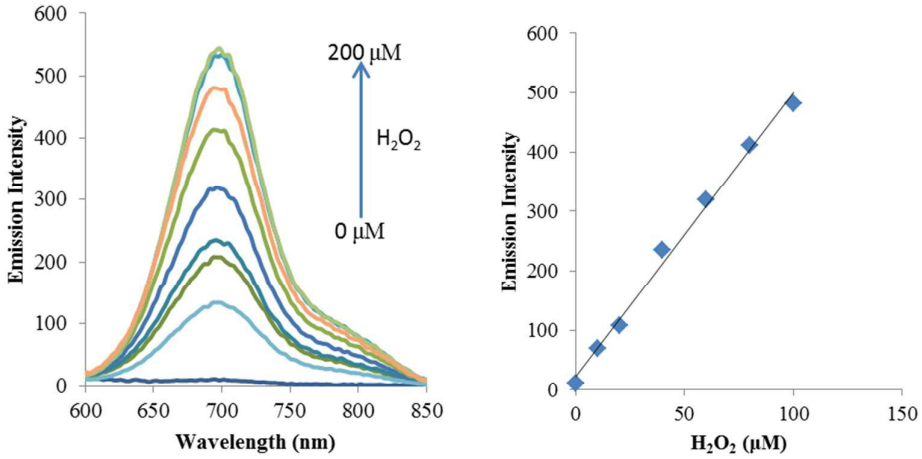


**Fig. 2** (a) Emission spectra of probe DCM-B1 in the presence of different equivalents of $H_2O_2$ (0, 0.5, 1.0, 2.0, 4.0, 6.0, 8.0, 10.0, 15.0, 20.0 eq, 30 min) excited at 560 nm; (b) A linear correlation between emission intensities and concentrations of $H_2O_2$.

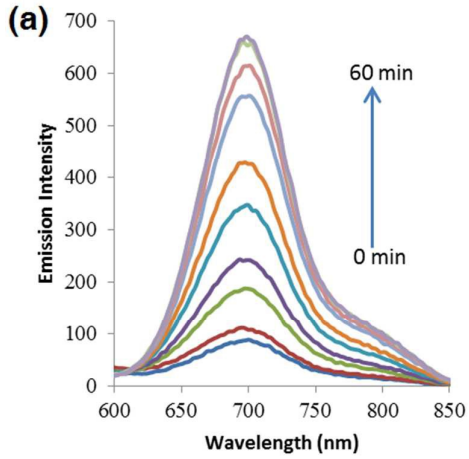


**Fig. 3** (a) The change in the emission spectra of DCM-B1 (5 μM) with time after addition of 100 μM $H_2O_2$; (b) The change in the emission spectra of DCM-B2 (5 μM) with time after addition of 100 μM $H_2O_2$; (c) Time-dependent fluorescence changes of DCM-B1 and DCM-B2 (5 μM) upon addition of $H_2O_2$ (100 μM).

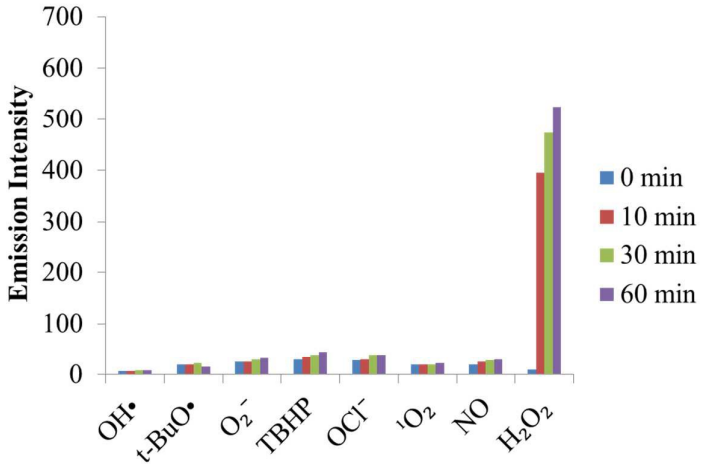


**Fig. 4** Fluorescence intensity of 5 μM DCM-B2 to the testing species in PBS buffer solution (20 mM, 50% DMSO, pH 7.4) at 700 nm excited at 560 nm. Bars represent fluorescence intensity during 0, 10, 30 and 60 min after addition of various compounds excited at 560 nm.

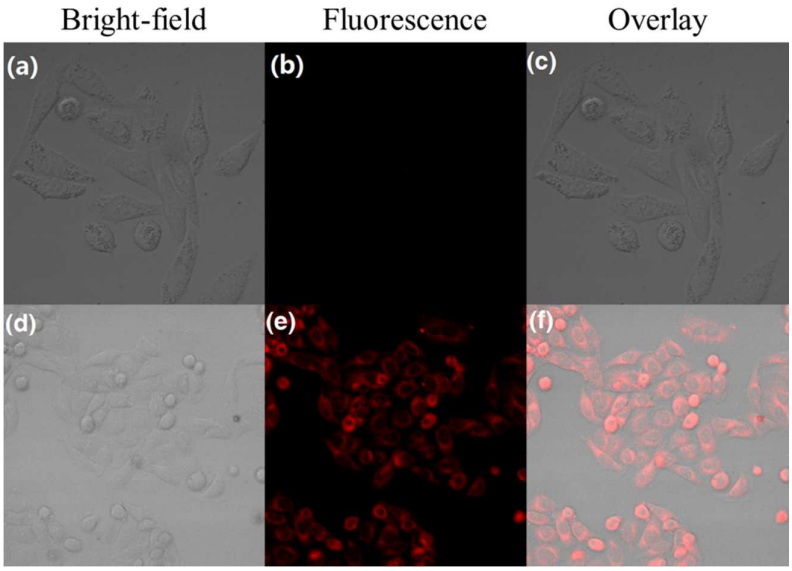


**Fig. 5** Fluorescence and bright-field images of MCF-7 cells. (a) Bright-field image image of cells incubated with DCM-B2 (10 μM) for 30 min; (b) Fluorescence image of cells shown in panel (a); (c) overlay image of (a) and (b); (d) Bright-field image of cells pretreated with DCM-B2 (10 μM) and then incubated with $H_2O_2$ (μM) for 30 min; (e) Fluorescence image of cells shown in panel (d); (f) overlay image of (d) and (e). Excitation was provided at 568 nm.

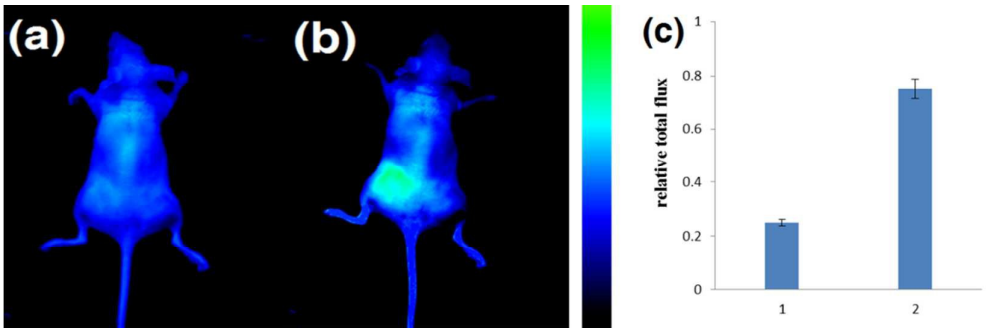


**Fig. 6** Fluorescence imaging of exogenous $H_2O_2$ activity with DCM-B2 in nude mice. (a) Mice injected s.p. with DCM-B2 (100 μL in 1:9 DMSO/saline v/v) for 40 min; (b) mice injected s.p. with DCM-B2 (100 μL in 1:9 DMSO/saline v/v), and then loaded with $H_2O_2$ (2 mM, 100 μL in saline) for 30 min; (c) quantification of total photon flux from the region of interest for each group. Images constructed from the 700 nm fluorescence window, $\lambda_{ex}$ = 660 nm.